

This discussion paper is/has been under review for the journal The Cryosphere (TC).
Please refer to the corresponding final paper in TC if available.

Sea ice melt pond fraction estimation from dual-polarisation C-band SAR – Part 2: Scaling in situ to Radarsat-2

R. K. Scharien, K. Hochheim, J. Landy, and D. G. Barber

Centre for Earth Observation Science, Faculty of Environment Earth and Resources,
University of Manitoba, Winnipeg, Manitoba, USA

Received: 19 December 2013 – Accepted: 6 January 2014 – Published: 27 January 2014

Correspondence to: R. K. Scharien (randall.scharien@umanitoba.ca)

Published by Copernicus Publications on behalf of the European Geosciences Union.

TCD

8, 845–885, 2014

Sea ice melt pond fraction estimation – Part 2

R. K. Scharien

Title Page

Abstract

Introduction

Conclusions

References

Tables

Figures

◀

▶

◀

▶

Back

Close

Full Screen / Esc

Printer-friendly Version

Interactive Discussion



Abstract

Observed changes in the Arctic have motivated efforts to understand and model its components as an integrated and adaptive system at increasingly finer scales. Sea ice melt pond fraction, an important summer sea ice component affecting surface albedo and light transmittance across the ocean-sea ice-atmosphere interface, is inadequately parameterized in models due to a lack of large scale observations. In this paper, results from a multi-scale remote sensing program dedicated to the retrieval of pond fraction from satellite C-band synthetic aperture radar (SAR) are detailed. The study was conducted on first-year sea (FY) ice in the Canadian Arctic Archipelago during the summer melt period in June 2012. Approaches to retrieve the subscale FY ice pond fraction from mixed pixels in RADARSAT-2 imagery, using in situ, surface scattering theory, and image data are assessed. Each algorithm exploits the dominant effect of high dielectric free-water ponds on the VV/HH polarisation ratio (PR) at moderate to high incidence angles (about 40° and above). Algorithms are applied to four images corresponding to discrete stages of the seasonal pond evolutionary cycle, and model performance is assessed using coincident pond fraction measurements from partitioned aerial photos. A RMSE of 0.07, across a pond fraction range of 0.10 to 0.70, is achieved during intermediate and late seasonal stages. Weak model performance is attributed to wet snow (pond formation) and synoptically driven pond freezing events (all stages), though PR has utility for identification of these events when considered in time series context. Results demonstrate the potential of wide-swath, dual-polarisation, SAR for large-scale observations of pond fraction with temporal frequency suitable for process-scale studies and improvements to model parameterizations.

1 Introduction

A decline in Arctic sea ice thickness over the past several decades (Kwok and Rothrock, 2009) has been linked in recent years to a predominantly seasonal sea ice regime. Be-

TCD

8, 845–885, 2014

Sea ice melt pond fraction estimation – Part 2

R. K. Scharien

Title Page

Abstract

Introduction

Conclusions

References

Tables

Figures

◀

▶

◀

▶

Back

Close

Full Screen / Esc

Printer-friendly Version

Interactive Discussion



ginning around 2007, the winter volume of sea ice in the Arctic became dominated by thinner first-year (FY) ice, rather than thicker multiyear (MY) ice (Kwok et al., 2009). A FY ice dominant regime has a greater annual areal fraction of melt ponds during summer melt, due to a relative lack of topographical controls on melt water flow compared to MY ice (Fetterer and Untersteiner, 1998; Barber and Yackel, 1999; Eicken et al., 2002, 2004; Freitag and Eicken, 2003; Polashenski et al., 2012). Melt ponds have much lower albedo (~ 0.2 – 0.4) than the surrounding ice cover (~ 0.6 – 0.8) (Perovich, 1996; Hanesiak et al., 2001b), which promotes shortwave energy absorption into the ice volume and accelerates ice decay (Maykut, 1985; Hanesiak et al., 2001a). Heat uptake by pond covered ice increases the rate at which its temperature related brine volume fraction increases to the $\sim 5\%$ threshold, the point at which the fluid permeability threshold is crossed (Golden et al., 1998) and vertical biogeochemical material exchange of the full ice volume with the underlying ocean becomes possible (see Vancoppenolle et al., 2013, for a review). Melt ponds transmit light to the underlying ocean at an order of magnitude higher rate than bare ice (Inoue et al., 2008; Light et al., 2008; Ehn et al., 2011; Frey et al., 2011), which leads to warming (Perovich et al., 2007) and stimulates under-ice primary production (Mundy et al., 2009; Arrigo et al., 2012) in the upper ocean layer. Increased ocean surface warming has been linked to subsequent reductions in ice volume due to its effect on the timing of seasonal melt onset and fall-freeze up (Laxon et al., 2003; Perovich et al., 2007). The proliferation of melt ponds is also related to the atmospheric deposition, and discharge into the ocean, of contaminants such as organochlorine pesticides (Pucko et al., 2012) and higher nutrient concentrations (Lee et al., 2012).

Understanding the role of melt ponds in large scale climatological and biogeochemical processes, improving weather forecast models, and conducting climate-cryosphere process studies introduce the challenge of upscaling the results of field studies to regional and greater scales. Improvements to parameterizations of melt pond evolution have led to more comprehensive, physically based, sea ice albedo schemes used in climate model simulations (Taylor and Feltham, 2004; Lüthje et al., 2006; Køltzow, 2007;

TCD

8, 845–885, 2014

Sea ice melt pond fraction estimation – Part 2

R. K. Scharien

Title Page

Abstract

Introduction

Conclusions

References

Tables

Figures

◀

▶

◀

▶

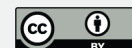
Back

Close

Full Screen / Esc

Printer-friendly Version

Interactive Discussion



Skyllingstad et al., 2009; Flocco et al., 2010) and a greater understanding of ice-albedo feedbacks (Holland et al., 2012). However the parameterizations are based on limited field observations that do not account for the horizontal heterogeneity of ice types and pond fractions. The pond fraction on a mixture of FY and MY ice may vary locally from 10–70 % at a snapshot in time (e.g. Derksen et al., 1997; Eicken et al., 2004; Polashenski et al., 2012). Over time, variations at one location up to 50 % are typical (Perovich and Polashenski, 2012), with changes greater than 75 % observed on the smoothest FY ice (Scharien and Yackel, 2005; Hanesiak et al., 2001b). Diurnal variations as high as 35 % have been observed on FY ice (Scharien and Yackel, 2005).

Satellite scale observations of melt pond properties require improvements to retrieval methods. Unmixing algorithms have been developed for estimating pond fraction from multispectral optical data (Markus et al., 2003; Tschudi et al., 2008; Rösel et al., 2012) and applied to a basin-scale analysis of pond fraction patterns using MODIS sensor data from 2000–2011 (Rösel and Kalschke, 2012). Optical approaches are limited by assumptions made regarding the predefined spectral behaviour of surface types open water, melt ponds, and snow/ice (Zege et al., 2012). The frequency of optical observations are also limited by persistent stratus cloud cover over the Arctic during summer (Inoue et al., 2005). Passive and active microwave radiometers and scatterometers provide Arctic-wide coverage of summer ice regardless of cloud cover and weather conditions. Data from these sensors have been used to identify pond formation (Comiso and Kwok, 1996; Howell et al., 2006), though their low resolution (several kilometres) and vulnerability to signal contamination by land and open water (Heygster et al., 2012) make quantitative melt pond retrievals problematic. Synthetic Aperture Radar (SAR) data has been investigated for its utility in providing synoptic scale melt pond information. SAR is an all-weather, active microwave, backscatter data source that provides much higher spatial resolution (30 m or greater) compared to radiometers and scatterometers, though at much reduced swaths. Several studies focused on C-band frequency backscatter coefficients measured by a single transmit-receive polarisation channel, e.g. from SARs ERS-1 (VV) and RADARSAT-1 (HH), to identify the onset of

Sea ice melt pond fraction estimation – Part 2

R. K. Scharien

Title Page

Abstract

Introduction

Conclusions

References

Tables

Figures

◀

▶

◀

▶

Back

Close

Full Screen / Esc

Printer-friendly Version

Interactive Discussion



ponding and for proxy estimates of sea ice albedo and pond fraction (Jeffries et al., 1997; Yackel and Barber, 2000; Hanesiak et al., 2001a). Single polarisation backscatter intensity variations caused by variable wind stress on pond surfaces imposes the need for ancillary wind speed measurements to aid retrievals (Comsio and Kwok, 1996; Barber and Yackel, 1999; De Abreu et al., 2001). Using in situ measured C-band polarimetric backscatter from pond covered Arctic FY ice, Scharien et al. (2012) demonstrated that the polarimetric ratio (PR) behaved independently of surface roughness and that the PR response of individual pond and bare ice samples was consistent with Bragg behaviour. The PR is a ratio of the linear, co-polarisation, transmit-receive (VV and HH) channels measurable by dual-polarised or polarimetric radars. As outlined in more detail in Sect. 2.2, the PR of a Bragg surface is independent of surface roughness and responsive to the dielectric constant (Fung, 1994). Scharien et al. (2012) found the PR of high dielectric free water ponds was much greater than bare ice, and they suggested evaluating a PR-based approach for the retrieval of pond information (e.g. pond formation, pond fraction evolution) from satellite SAR, combined with more rigorous evaluation of the roughness characteristics of the surface in relation to Bragg scattering model theory.

In Part 1 of this study, detailed in situ surface roughness measurements of advanced melt FY ice pond and bare ice features were compared to the rough surface validity limit of the Bragg model at C-band frequency (Scharien et al., 2014; this issue). This was done within the framework of our working hypothesis: as defined by Bragg model theory, FY ice melt pond fraction is retrievable from PR measured at C-band frequency. Part 1 demonstrated that bare ice falls within the Bragg validity limit, while the roughest ponds exceed the limit. Establishing a wind speed threshold for the roughest ponds is unsatisfactory, as morphological factors also contribute to pond roughness. The dominant factor is fetch, which for a spatially distributed mixture of ponds and bare ice effectively increases when the wind direction is aligned with the long axes of ponds. Approximate 10 m wind speed thresholds of 6.4 and 8.0 ms⁻¹ are provided as a guideline, depending on the presence or absence of morphological factors, respectively.

Sea ice melt pond fraction estimation – Part 2

R. K. Scharien

Title Page

Abstract

Introduction

Conclusions

References

Tables

Figures

◀

▶

◀

▶

Back

Close

Full Screen / Esc

Printer-friendly Version

Interactive Discussion



Though the Bragg limit of FY ice ponds can be exceeded, the scale of analysis in Part 1 represents a significant oversampling in spatial and temporal dimensions, requiring analysis of distributed pond and ice data in satellite SAR.

In this paper, Part 2, a satellite SAR scale evaluation of our working hypothesis is conducted by combining RADARSAT-2 (RS-2) derived backscatter statistics with coincident aerial photography (AP). Though emphasis is placed on the PR, linear co- and cross-polarisation (VV, HH, and HV) and cross-polarisation ratio (HV/HH) statistics are included for enhanced interpretation. Within this framework the following objectives are addressed: (1) to synthesize calibrated dual-polarisation C-band frequency RADARSAT-2 backscatter statistics over undeformed FY ice during the ponding season, and (2) to evaluate novel approaches for the retrieval of FY melt pond fraction using the PR. The first objective addresses spatial and temporal aspects of RS-2 backscatter and pond fraction. Backscatter statistics and AP derived pond fractions are compared during discrete melt pond evolutionary stages, demarcated by Eicken et al. (2002) and described in Sect. 2.1. This provides the basis for the second objective, which directly addresses the working hypothesis. Section 2.2 describes the Bragg scattering model as it pertains to PR based unmixing of pond fraction. Methods used to acquire and process the experimental dataset, and three experimental methods to retrieve pond fractions from calibrated RS-2 PR bands are described in Sect. 3. Results in Sect. 4 are ordered as follows: a seasonal description of backscatter statistics and pond fraction evolution (Sect. 4.1); a comparison of spatially distributed polarisation ratios and pond fractions along each AP flight lines (Sect. 4.2); and an evaluation of RS-2 retrieved and AP derived pond fractions using statistics RMSE and bias (Sect. 4.3). Pertinent findings and limitations are discussed in Sect. 5, before the main results are recalled and conclusions made in Sect. 6.

Sea ice melt pond fraction estimation – Part 2

R. K. Scharien

[Title Page](#)[Abstract](#)[Introduction](#)[Conclusions](#)[References](#)[Tables](#)[Figures](#)[◀](#)[▶](#)[◀](#)[▶](#)[Back](#)[Close](#)[Full Screen / Esc](#)[Printer-friendly Version](#)[Interactive Discussion](#)

2 Background

2.1 Stages of pond evolution

In order to simplify the dynamic nature of ponding, various sub-stages have been identified. These are either based on the thermodynamic (ablation) state of the ice volume (Hanesiak et al., 2001a; Perovich et al., 2007), or the evolution of surface hydrology (Eicken et al., 2002). The stages outlined in Eicken et al. (2002) in an analysis of flow rates and transport pathways on summer FY and MY in the northern Chukchi Sea, are used in this study. These staged, hereafter the “Eicken stages”, provide a logical coupling between evolving surface features and dominant microwave backscatter mechanisms.

During the Ponding Stage I, the melting snow cover provides a rapid influx of melt water which laterally spreads over a large area (high pond fraction) on undeformed first-year ice. Past observations have shown that the seasonal peak in pond fraction on FY ice occurs as melt water from the rapidly ablating snow cover is retained by an impermeable ice cover (see summary of published data in Polashenski et al., 2012). As there are almost no topographical controls on melt water flow, ponds spread laterally so that the peak fraction typically reaches > 0.5 (Eicken et al., 2004). Ponding Stage II begins when the snow cover has ablated and the pond fraction is driven by the balance between melt rate (rise in pond fraction) and lateral flows through cracks and seal holes (drop in pond fraction). Pond fraction during this stage is driven by a balance between the intensity of melt, which controls meltwater production, and lateral and vertical fluxes of meltwater, which control meltwater drainage (Eicken et al., 2002). Ponding Stage III is demarcated by hydraulic connectivity between the ice and the ocean, and the vertical, in addition to lateral, transport of water through macroscopic holes in the ice. During this stage vertical pathways between the ice cover and ocean form, leading to vertical drainage and lower pond fractions when pond surfaces are above freeboard, and increased seawater flooding and higher pond fractions when they reach sea level. Due to enhanced drainage, Stage III is also referred to the pond drainage stage.

Sea ice melt pond fraction estimation – Part 2

R. K. Scharien

Title Page

Abstract

Introduction

Conclusions

References

Tables

Figures

◀

▶

◀

▶

Back

Close

Full Screen / Esc

Printer-friendly Version

Interactive Discussion



2.2 Bragg scattering model

For a surface comprising roughness features that are small relative to the incident radar wavelength, its linear polarisation backscatter can be described by the small perturbation or Bragg model (Fung, 1994). A Bragg model surface is defined by the smooth surface roughness validity criterion $ks < 0.3$, where $k = 2\pi/\lambda$ and s is the surface rms-height. The scattering mechanism is single (surface) scattering and, as described in Hajnsek et al. (2003), its polarimetric backscatter behaviour is described by a scattering matrix $[\mathbf{S}]$:

$$[\mathbf{S}] = \begin{bmatrix} S_{hh} & S_{hv} \\ S_{vh} & S_{vv} \end{bmatrix}, \quad (1)$$

where the subscripts refer to the transmit and receive polarizations which are horizontal (h) and vertical (v) for the linear basis. For a Bragg surface, Eq. (1) can be modified as follows:

$$[\mathbf{S}] = m_s \begin{bmatrix} R_{hh}(\theta, \varepsilon_r) & 0 \\ 0 & R_{vv}(\theta, \varepsilon_r) \end{bmatrix}, \quad (2)$$

where m_s is the backscatter amplitude and R_{hh} and R_{vv} are Bragg scattering coefficients:

$$R_{hh} = \frac{\cos(\theta) - \sqrt{\varepsilon_r - \sin^2(\theta)}}{\cos(\theta) + \sqrt{\varepsilon_r - \sin^2(\theta)}}, \quad (3)$$

$$R_{vv} = \frac{(\varepsilon_r - 1) \left\{ \sin^2(\theta) - \varepsilon_r [1 + \sin^2(\theta)] \right\}}{\left(\varepsilon_r \cos(\theta) + \sqrt{\varepsilon_r - \sin^2(\theta)} \right)^2}. \quad (4)$$

TCD

8, 845–885, 2014

Sea ice melt pond fraction estimation – Part 2

R. K. Scharien

Title Page

Abstract

Introduction

Conclusions

References

Tables

Figures

◀

▶

◀

▶

Back

Close

Full Screen / Esc

Printer-friendly Version

Interactive Discussion



From Eqs. (2) and (3), the ratio of Bragg coefficients (R_{vv}/R_{hh}) is independent of surface roughness and dependent only on the radar incidence angle θ and the surface complex permittivity or dielectric constant ε_r . The ratio is equivalent to the PR derived from VV and HH transmit-receive radar scattering coefficients (σ°) recorded by an imaging radar or scatterometer:

$$PR = \frac{\sigma_{vv}^\circ}{\sigma_{hh}^\circ}. \quad (5)$$

On the one hand, knowledge of the permittivity of a Bragg surface enables the estimation of the PR. Conversely, a PR model may allow the simple retrieval of a geophysical parameter on the basis of changes in its bulk permittivity. Detectable changes in the bulk permittivity are typically dominated by the presence of a high dielectric such as water or brine. Considering a pond covered sea ice surface, a low dielectric sea ice host with $\varepsilon_i = 3.11 + 0.208i$ is covered with varying fractions of high dielectric ponds with $\varepsilon_w = 67.03 + 35.96i$. A mixture modelling approach can be used to estimate the surface ε_r corresponding to a horizontally distributed mixture of ice and ponds (Ulaby et al., 1986):

$$\varepsilon_r = \varepsilon_h + v_w(\varepsilon_w - \varepsilon_h). \quad (6)$$

From this, Eqs. (3) and (4) are then used to create a PR model for pond fraction (Fig. 1). Figure 1 illustrates the use of a PR model for the estimation of parameters related to the formation, pond fraction evolution, and drainage of melt pond from a sea ice surface which conforms to the Bragg surface roughness limit. Ponds are more easily detected at larger θ and when the pond fraction is high, as denoted by a relative increase in PR by several decibels (dB) compared to smaller θ and lower pond fractions. It follows that a pond fraction may be retrieved from the PR at a fixed θ , again provided the θ is high enough to enable a response to the permittivity contrast between ponds and sea ice.

Sea ice melt pond fraction estimation – Part 2

R. K. Scharien

Title Page

Abstract

Introduction

Conclusions

References

Tables

Figures

◀

▶

◀

▶

Back

Close

Full Screen / Esc

Printer-friendly Version

Interactive Discussion



3 Methods

3.1 Data collection

Data were collected during the Arctic-Ice Covered Ecosystem in a Rapidly Changing Environment (Arctic-ICE) field project from May – June 2012. Arctic-ICE is an interdisciplinary project with focus on biogeophysical processes occurring at the ocean-sea ice-atmosphere (OSA) interface during the spring-summer snow melt and ponding periods. The project was conducted on the relatively undeformed, landfast, FY ice in the central Canadian Arctic Archipelago, adjacent to Resolute Bay, Nunavut. Proximity to Resolute Bay enabled access to the nearby airport and the coupling of in situ data with aerial photography (AP) flights flown over the study site. Figure 2 shows a map of the field study site location, along with the configuration of AP survey lines over the field site (hereafter Field) and Parry Sound (hereafter Parry). Also included in Fig. 2 are the outlines of the RS-2 acquisitions acquired for this study (described in detail below).

AP surveys were conducted to capture digital imagery of the ice surface and quantify relative fractions of pond, ice, and open water. During each survey, a set of lines were flown over Parry at an altitude of 1542 m (~ 5000 ft), followed by lines over the study site at 610 m (~ 2000 ft). Images were captured using a Canon G10 camera mounted to an open hatch in the rear of a fixed wing DHC-6 Twin Otter aircraft. The camera was operated in time-lapse mode, with camera settings and capture rate controlled using a laptop and proprietary software. At 1542 m flying height, images cover an estimated 1872 m swath with 0.54 m pixel size; at 610 m flying height the swath is 749 m and pixel size 0.22 m. Adjustments to the time-lapse capture rate were made during flights to ensure a regular 10 % overlap, for example when ground speed or altitude variations occurred. A time-synched GPS on the aircraft was used to log x , y , and z position data at 1 s resolution, which enabled image registration (geotagging) during post-processing. Image data from four AP surveys are used in this study, chosen due to their proximity to RS-2 overpasses. Dates, start times, and identifiers for each of

TCD

8, 845–885, 2014

Sea ice melt pond fraction estimation – Part 2

R. K. Scharien

Title Page

Abstract

Introduction

Conclusions

References

Tables

Figures

◀

▶

◀

▶

Back

Close

Full Screen / Esc

Printer-friendly Version

Interactive Discussion



these flights are: 13 June 2012 T 22:55 Z (AP1), 22 June 2012 T 01:43 Z (AP2), 24 June 2012 T 00:08 Z (AP3), and 29 June 2012 T 14:09 Z (AP4).

C-band frequency RS-2 SAR images were acquired in fine beam quad-polarimetric (quad-pol) mode over the study site, including Parry, during the Arctic-ICE 2012 study.

5 Each acquisition comprises a fully polarimetric (HH + VV + HV + VH and inter-channel phase information) dataset, with a nominal 5.2 by 7.7 m resolution in range and azimuth, and a 25 by 25 km image size (MDA, 2009). Despite a relatively small swath width, the low noise equivalent sigma zero (NESZ) of the quad-pol mode, nominally -36.5 ± 3 dB, makes it an essential tool for experimental studies of low intensity targets
10 such as summer sea ice. In addition, our working hypothesis requires the collection of scenes acquired at shallow (high) incidence angles with relatively lower backscatter levels. Of the 31 selectable beams available across the full 18° to 49° incidence angle range available in fine quad-pol mode (1° to 2° width each), approximately the last 12 (39° to 49°) are applicable. Extended 75 by 25 km acquisitions were made over Parry
15 by tasking four adjacent scenes in the along-track direction and later mosaicking them. Four RS-2 acquisitions over Parry were collected for this study: a descending pass prior to the onset of ponds on 12 May 2012 T 12:51 Z (R1), ascending passes during ponding on 13 June 2012 T 23:54 Z (R2) and 24 June 2012 T 00:02 Z (R4), and a descending pass during late ponding on 28 May 2012 T 12:51 Z (R5). A single ascending
20 pass during ponding at Field on 20 June 2012 T 23:50 Z (R3) was also acquired. Each of these scenes has a shallow incidence angle (41 to 44°) and, with the exception of R3, falls within 3 h of an AP survey. R3 was a local evening overpass, with its corresponding survey AP2 flown approximately 24 h later.

25 Meteorological variables air temperature and wind speed, as well as weather observations, were obtained from the WMO standard Environment Canada (EC) weather station located at Resolute Bay airport ($74^\circ 42' 57.005''$ N, $94^\circ 58' 59.007''$ W), about 12 km from Field. EC data are used for assessment of general conditions associated RS-2 acquisitions, providing consistency as overpasses extended beyond the duration of the field study. On a case-by-case basis, hourly in situ micrometeorological data recorded

TCD

8, 845–885, 2014

Sea ice melt pond fraction estimation – Part 2

R. K. Scharien

Title Page

Abstract

Introduction

Conclusions

References

Tables

Figures

◀

▶

◀

▶

Back

Close

Full Screen / Esc

Printer-friendly Version

Interactive Discussion



at Field are used. Air temperature ($\pm 0.1^\circ\text{C}$) and relative humidity ($\pm 0.8\%$) at 2 m were sampled using a Rotronic Hygroclip 2 Probe. Surface skin temperature ($\pm 0.5^\circ\text{C}$) was measured using an Apogee SI-111 Infrared Radiometer. Incoming longwave and short-wave radiation ($\pm 10\%$) were measured using a Kipp & Zonen CNR-4 Net Radiometer.

- 5 A thermistor string mounted in a melt pond provided water temperature readings at 0.5 cm vertical intervals.

3.2 Data processing

Each complex polarimetric RS-2 dataset was processed to a final calibrated and projected product including image bands of VV, HH, and HV polarisation backscatter coefficients, polarisation ratios PR (VV/HH) and PR_x (HV/HH), and local incidence angle. Pre-processing included undersampling the raw data by a factor of 2 in range and azimuth, in order to remove correlated adjacent pixels resulting from the SAR image formation process. A 5 by 5 boxcar speckle filter was applied to reduce the speckle component while preserving image statistics (Oliver and Quegan, 2004). Raw data were then converted to ground range coordinates, calibrated to sigma nought, and projected to a common map projection at 12 m pixel spacing. This yielded an estimated 20 equivalent number of looks (ENL) at 44° incidence angle, based on statistics derived from user-selected homogeneous open water targets. The World Vector Shoreline (WVS), a vector data file at a nominal scale of 1 : 250 000 and provided by the NOAA National Geophysical Data Center (Soluri and Woodson, 1990), was applied to mask out land within scenes.

A correction for additive noise was applied to RS-2 data before calculating PR. The methods was based on Johnsen et al. (2008), who found that the subtraction of additive noise improved calculations of PR from wind roughened ocean at high incidence angles. A polynomial was fitted to the range, or incidence angle (θ), dependent additive noise provided in RS-2 product headers and the noise corrected PR band from each

TCD

8, 845–885, 2014

Sea ice melt pond fraction estimation – Part 2

R. K. Scharien

Title Page

Abstract

Introduction

Conclusions

References

Tables

Figures

◀

▶

◀

▶

Back

Close

Full Screen / Esc

Printer-friendly Version

Interactive Discussion



scene was determined as:

$$PR = 10 \times \log_{10} \left[\frac{\sigma_{vv}^{\circ} - (A\theta^4 - B\theta^3 + C\theta^2 - D\theta + F)}{\sigma_{hh}^{\circ} - (A\theta^4 - B\theta^3 + C\theta^2 - D\theta + F)} \right], \quad (7)$$

with coefficients A-F derived for each fine quad-pol (FQ) product. The additive noise was not subtracted out of the HV and HH channels before calculating the PR_x since we found that, as did Vachon and Wolfe (2011) when comparing PR_x to ocean wind speed, this step did not improve subsequent correlations an information retrievals as it did for PR.

Digital images from AP survey lines were partitioned into scenes composed of three classes: ice, melt pond, and open water, using a decision-tree classification approach. This method was based on Tschudi et al. (2001), who demonstrated the effectiveness of combining the RGB band reflectance similarities and contrasts of these features in a simple classifier. Simply, the spectral response curves of ice and open water across all RGB bands are flat, but separable in terms of magnitude, as ice is high (bright) and open water low (dark). Ponds, on the other hand, exhibit a strong contrast between red and blue channels. Decision tree nodes corresponding to each survey line were constructed in order to account for variations in ambient lighting conditions. In some cases this was done within a single survey line. After partitioning, images from high- and low-altitude survey lines were trimmed to estimated ground coverages of 900 by 900 m and 750 by 750 m, respectively, which eliminated image edges with poor radiometric resolution and improved the performance of classifiers.

A classifier performance evaluation was conducted by comparing the derived relative fractions of features from a set of partitioned scenes to fractions calculated by an expert using a manual approach. The manual approach involved using a K-means un-supervised classification algorithm and iteratively merging $n \gg 3$ classes to $n = 3$ classes using a top-down approach. The average pond fraction classification error was determined to be $\pm 3\%$. A demonstration of the decision-tree classifier on a scene comprising ponds, ice, and open water is given in Fig. 3.

Sea ice melt pond fraction estimation – Part 2

R. K. Scharien

Title Page

Abstract

Introduction

Conclusions

References

Tables

Figures

◀

▶

◀

▶

Back

Close

Full Screen / Esc

Printer-friendly Version

Interactive Discussion



Surface class statistics from AP survey lines AP1 to AP4 were matched to coincident SAR statistics from RS-2 acquisitions R2 to R5 (R1 was acquired prior to ponding) using the location information associated with each partitioned image. A 75 by 75 pixel square centred on the x , y position of a partitioned AP image was used to extract coincident SAR statistics for each co-located position along the high altitude survey lines over Parry. A 60 by 60 pixel box was used for low altitude survey lines over Field. To eliminate the influence of open water on backscatter statistics, instead of ponds, partitioned AP images with $> 1\%$ open water were removed from the analysis. Finally, sample pairs were reduced by a factor of 2 to eliminate the potential for overlap and reduce the influence of spatial autocorrelation.

3.3 Pond fraction retrieval

Three approaches for retrieving pond fraction from calibrated RS-2 PR bands were tested. A grid composed of 7.5 by 7.5 km cells was overlaid on the study site, and collocated SAR and AP derived pond fractions corresponding to each of the four AP surveys were aggregated. This scale was chosen as it provides a good compromise between the high spatial resolution RS-2 imagery and high-resolution regional scale climate models (Maslowski et al., 2011). Statistics of linear association (r^2), bias, and root-mean-square error (RMSE) were used to evaluate model performances.

The first retrieval method is based on modelled incidence angle dependent functions of PR for ponds, derived from in situ C-band scatterometer observations from the same study and detailed in Part 1. The following function:

$$PR = 1.320 + -0.103\theta + 0.004\theta^2, \quad (8)$$

describes the PR of a pure FY ice melt pond (pond fraction of 1) across the 25–60° incidence angle (θ) range. On the basis of an assumed ice PR of null from Part 1, combined with the assumption of linear mixing in the horizontal domain, a look-up-table was constructed for the retrieval pond fraction (0–1) from PR of a mixed pixel at a given incidence angle. The second method is also based on the assumption of

Sea ice melt pond fraction estimation – Part 2

R. K. Scharien

Title Page

Abstract

Introduction

Conclusions

References

Tables

Figures

◀

▶

◀

▶

Back

Close

Full Screen / Esc

Printer-friendly Version

Interactive Discussion



horizontal mixing of PR, this time with the Bragg model used for estimates of PR, as described in Sect. 2.2 and illustrated in Fig. 1. However the assumption of a null PR was also used for the Bragg based model, on the basis of the results presented in Part 1 and the documented presence of non-Bragg scattering mechanisms from the ice cover.

The third approach is based on cross-validation, where a sub-sample of the dataset is used to construct a predictive model, which is then applied to a set of data not used in the estimation. Full-resolution collocated data corresponding to AP2 and AP4 were used to create a linear model for the estimation of pond fraction (F_p) from PR:

$$F_p = 0.156 \cdot PR + 0.153 \text{ [dB]}. \quad (9)$$

This is not a true cross-validation approach since the model, created using full resolution data from AP2 and AP4, was applied to aggregated samples from AP2 and AP4. Though this introduces bias in the inversion process, the approach follows that used successfully to train models for wind speed retrievals from ocean backscatter and facilitate preliminary model performance assessment (e.g., Vachon and Wolfe, 2011).

4 Results

4.1 Seasonal evolution of pond coverage and SAR backscatter

Average VV, HH, HV, PR, and PR_x are shown along coincident average pond fractions in Table 1. Values from Parry site were derived from the area corresponding to the RS-2 image overlap region denoted in Fig. 2. Values from Field site were derived from the entire area within the 25 by 25 km RS-2 outline in Fig. 2. These data facilitate evaluation of the seasonal behaviour of backscatter and polarisation ratio levels relative to the Eicken stages, though slight variations due to incidence angle (44–49°) must be considered. A general assessment of backscatter levels relative to the NESZ of RS-

TCD

8, 845–885, 2014

Sea ice melt pond fraction estimation – Part 2

R. K. Scharien

Title Page

Abstract

Introduction

Conclusions

References

Tables

Figures

◀

▶

◀

▶

Back

Close

Full Screen / Esc

Printer-friendly Version

Interactive Discussion



2 (and other SARs) is also possible using the data in Table 1, particularly given the shallow incidence angles used.

Baseline scene R1 was acquired on 12 May, under relatively cold (winter) conditions and several weeks prior to ponding. Backscatter at all polarisations, as well as PR, are lower than during ponding, while PR_x is higher. R2 coincided with the observed Ponding Stage I at Field. An average pond fraction of 0.38 during R2 is lower than expected for a Stage I peak, as previously observed in the region (Yackel et al., 2000; De Abreu et al., 2001; Scharien and Yackel, 2005). This suggests the acquisition took place during the initial stage I upturn in pond fraction. Backscatter increases relative to R1 are attributed to stronger surface scattering contributions from wind-wave roughened ponds and wet snow, with the former caused by strong coincident wind forcing ($U_{10} = 11.9 \text{ ms}^{-1}$) from an approaching storm. A PR increase by several dB between R1 and R2 is consistent with a Bragg-like surface perturbation caused by ponds.

R3 and R4 were acquired over a four day period corresponding to Ponding Stage II at Field site, beginning one week after R2. The snow cover at Field had ablated, leaving discrete pond and bare ice patches. Pond fractions (> 0.5) are higher relative to R2. Backscatter at HH and HV polarisations increase relative to winter (R1) and Ponding Stage I (R2) periods. These increases are despite a significant reduction in wind stress over melt ponds compared to R2. Associated reductions in PR during Ponding Stage II point to enhanced contribution to backscatter from drained, low salinity, bare ice patches. Bare ice on FY ice has been observed to have lower volumetric moisture content in its near surface layer than wet snow, which results in increased HH and VV intensities and less polarisation diversity due to volume scattering contributions (Scharien et al., 2010).

Scene R5 was acquired during the beginning of Ponding Stage III, the final stage before complete decay and/or breakup. This assessment is based on visual evidence, from aerial photographs, of drained white ice and flooded zones containing dark melt holes (open water) rather than blue coloured ponds. Observations at Field site were

TCD

8, 845–885, 2014

Sea ice melt pond fraction estimation – Part 2

R. K. Scharien

Title Page

Abstract

Introduction

Conclusions

References

Tables

Figures

◀

▶

◀

▶

Back

Close

Full Screen / Esc

Printer-friendly Version

Interactive Discussion



not possible this late in the season. Based on Table 1, average backscatter and PR data are not distinguishable from Ponding Stage II.

4.2 Spatially distributed polarisation ratios and pond fractions

Profiles of spatially collocated polarisation ratio and pond fraction samples corresponding to each of the RS-2/AP survey pairs are shown in Fig. 4. Each of the AP surveys comprises a wide range of pond fractions, and the entire dataset covers a 0.08–0.90 range. Though the emphasis of this study is on PR, PR_x is included in Fig. 4 to provide additional insights on the polarisation behaviour of backscatter. Coefficients of determination (r^2) between polarisation ratios and pond fractions in Fig. 4 are significant at $\alpha = 0.01$ for each survey except for R2. Slopes of significant regression lines are all positive; increases in pond fraction lead to increases in PR and PR_x .

There are two noteworthy characteristics regarding the relationship between pond fraction and PR for R2 in Fig. 4. First, lack of association between variables is contrary to the Bragg model. Second, PR values are predominantly large (4–5 dB) along the survey even when pond fraction is low. From Table 1, the coincident U_{10} (11.9 ms^{-1}) is much greater than the threshold (8 ms^{-1}) for pond surface roughness, beyond which the Bragg roughness limit is exceeded at C-band (see Scharien et al., 2014; this issue). The PR tends to unity with increasing roughness once the Bragg limit is surpassed. Considering wind stress and pond roughness are spatially variable across the scene during acquisition, contribution to the lack of association between variables is expected. However, this does not explain high PR values. As it is Ponding Stage I, zones of wet snow and slush must be considered present. These features are expected to have intermediate permittivities compared to bare ice and ponds, which would cause higher PR than expected (see Sect. 2.2).

Contrasting relationships between polarisation ratios and pond fractions are observed between R3 and R4, both of which occurred during Ponding Stage II. For R3, the strength of association between PR and pond fraction (0.54) is stronger than between PR_x and pond fraction (0.27). For R4, the opposite occurs (0.30 compared to

TCD

8, 845–885, 2014

Sea ice melt pond fraction estimation – Part 2

R. K. Scharien

Title Page

Abstract

Introduction

Conclusions

References

Tables

Figures

◀

▶

◀

▶

Back

Close

Full Screen / Esc

Printer-friendly Version

Interactive Discussion



0.54). The PR range from R4 is also consistently damped, indicating a stationary process along the survey line, even in highly ponded areas. The damping of PR during R4 is examined in more detail using in situ data from the Field site over the 12 h period surrounding the acquisition (Fig. 5). Shown in Fig. 5a are meteorological variables air temperature (T_a), surface temperature (T_{sfc}), and downwelling longwave radiation (Q_L^\downarrow) recorded at the Field site. Figure 5b shows the temperature profile of an adjacent melt pond. Incoming longwave emissions are above 300 W m^{-2} and surface melt is occurring until 01:00Z, when longwave radiation loss and surface cooling occurs. The cooling effect on the melt pond is apparent after 02:00Z when, despite warmer air temperature, the entire pond is very close to the triple point of water. This suggests the possible formation of a frozen surface layer on the pond, behaviour which is consistent with the clearing of the low-level stratus cloud cover that was observed to be present over the Field site during the R4 coincident AP flight at 00:00Z. The cloud layer was observed during transit to and from the Parry site, as the flight path crossed the Field site (see Fig. 2). The same cloud cover was also present over the Parry site earlier in the day, as indicated by NOAA AVHRR infrared Channel 4 imagery analysed during flight planning protocols conducted at Resolute airport. Though not directly verified by data collected at Field site, earlier clearing over the Parry site likely induced a surface cooling by the time of the R4 acquisition. Surface cooling leads to less absorption and enhanced penetration of C-band energy within the drained upper layer of bare ice patches, introducing non-Bragg, volume, scattering (Scharien et al., 2010) and a breakdown in the pond fraction – PR relationship. As suggested by Fig. 5b, cooling also leads to the possible formation of a surface ice lid on ponds and a reduction in pond PR to values resembling bare ice (see Part 1). The enhanced relationship between PR_x and pond fraction during the R4 cooling event is also consistent with the formation of an ice lid on pond surfaces. A positive association between PR_x with ponds, seen along the survey line, points to the greater loss in HH intensity contribution to the ratio, relative to HV intensity contribution, caused by the loss of surface wind waves (see Part 1).

Sea ice melt pond fraction estimation – Part 2

R. K. Scharien

Title Page

Abstract

Introduction

Conclusions

References

Tables

Figures

◀

▶

◀

▶

Back

Close

Full Screen / Esc

Printer-friendly Version

Interactive Discussion



The strongest coefficient of determination between pond fraction and PR (0.59) is derived from R5, despite a mixture of drained ice and melt holes indicative of Ponding Stage III, combined with remnant Ponding Stage II areas observed in partitioned AP imagery. The lowest PR (~ 0 dB) during R5 also traces the minimum 0.08 pond fraction.

- 5 This indicates limited detectability of pond fractions below approximately 0.10 using PR across the 44–49° incidence angle range, behaviour which is consistent with the modelled behaviour of PR in Fig. 1.

4.3 Pond fraction retrievals

- Spatial patterns of retrieved melt pond fractions, created by globally applying Eq. (8) to the PR bands from the RS-2 dataset, are shown in Fig. 6. Each of the RS-2 scenes in Fig. 6 is displayed in a manner consistent with the map information provided in Fig. 2. Caution is noted regarding the interpretation of the R1 and R2. The former occurred prior to pond onset, while the latter was taken during Ponding Stage I when, as above, PR and pond fraction are not linearly associated. Nonetheless, the series clearly reflects the onset and development of ponds. It is immediately clear that Ponding Stage I is discernible from winter, despite the high wind speed and expected modulation of PR during the acquisition of R2. Considering the overlap in single polarisation backscatter intensities caused by variable wind stress over ponds, the PR is advantageous for identifying the onset of ponding. Scenes R3 to R5 illustrate the spatial and temporal variability in pond fraction during Ponding Stages II and III. A small polynya is also visible in the top portion of the Parry site, to the north of the elongated island (Truro Island), in scenes R2, R4, and R5. The open water of the polynya appears as an area with pond fraction $\rightarrow 1$. Its growth from approximately 2–5 km width is apparent in the series. Spatial variability in pond fraction and presence of the polynya are further illustrated by visual inspection of the R5 acquisition compared to a cloud-free Landsat-7 ETM+ scene acquired on the same day (Fig. 7). Overall consistency between the two scenes is observed, as areas of high and low ponds fractions in R5 are coincident to dark-blue and white portions in the Landsat-7 scene.

Deviations between observed and retrieved pond fractions from downscaled (7.5 km grid cell) scenes, using the three retrieval methods tested in this study, are shown in Fig. 8. Coefficients of determination between observed and cross-validation modelled pond fractions are also shown in Fig. 8. Statistics RMSE and bias for all three retrieval methods are given in Table 2. A positive bias and large RMSE is evident over R2 using all three retrieval methods. This can be attributed to the contribution of wet snow/slush to higher than estimated PR in the scene (larger than expected surface permittivity). On the other hand, a negative bias and larger RMSE caused by the freezing of ponds is evident for all three retrieval methods applied to R4. Retrievals over R3 and R5 generally exhibit very small or negative bias. In cases of negative bias, it is attributed to the enhanced contribution of non-Bragg scattering mechanisms from bare ice which is present during ponding stages II and III. This mechanism results in a damping of PR and pond fraction underestimations. It was only effectively accounted for by the cross-validation model, created using RS-2 data.

Model comparison is restricted to scenes R3 and R5 due to low RMSE and bias associated with these acquisitions. The Cscat model generally underestimates pond fractions. As detailed in Part 1, the sampling strategy used to obtain in situ backscatter measurements and train the Cscat PR model was biased towards lower PR relative to that which are likely to occur in RS-2 data. In situ data collection strategy aimed at maximizing the impact of wind-wave roughness on backscatter parameters, in order to document the limits of these parameters in relation to wind stress and wave energy. A disproportionate number of Cscat samples were collected at the upwind radar orientation, the only orientation at which PR was negatively correlated with wind speed. Given that data acquired at all wind speeds were used in the Cscat model, this likely contributed to a lower estimate of PR. The modified Bragg model, with the PR contribution from ice set to null, has a lower RMSE (0.07–0.11) range than the Cscat model (0.07–0.15) over scenes R3 and R5. The cross-validation retrieval method has the lowest RMSE (0.07) and negligible bias, which is to be expected considering the use of

Sea ice melt pond fraction estimation – Part 2

R. K. Scharien

Title Page

Abstract

Introduction

Conclusions

References

Tables

Figures

◀

▶

◀

▶

Back

Close

Full Screen / Esc

Printer-friendly Version

Interactive Discussion



RS-2 data to create the model. The use of RS-2 also had the benefit of input data from across the entire study domain.

5 Discussion

Several factors point to the key role of C-band SAR in coming efforts to understand and model the Arctic environment as a complex and adaptive system at increasingly finer scales. First, coupling between the physical and thermodynamic evolution of snow-covered sea ice and SAR signatures is already well-established outside of the ponding period due to detailed in situ characterizations of physical and electromagnetic properties, and microwave interactions (e.g. Livingstone et al., 1987; Drinkwater, 1989; Barber, 2005; Perovich et al., 1998). Second, several SAR missions are either operational or nearing launch phases, including future multi-sensor constellations ESA Sentinel-1 (Torres et al., 2012) and Radarsat Constellation Mission (Flett et al., 2009). These missions will increase the revisit frequency in polar regions to sub-daily scale while providing wide swath dual-polarisation and compact polarimetric modes. Finally, SAR sensors operating in other frequencies, e.g. L-band ALOS PalSAR-2 and X-band TerraSAR-X, provide greater information content through frequency diversity. Despite its potential, the application of SAR in comprehensive EO-based sea ice process monitoring and modelling frameworks lags achievements at the in situ scale. This lag is due in part to uncertainties imposed by the spatial heterogeneity of sea ice, combined with variable radar parameters such as incidence angle and polarisation, when scaling to the SAR scale. Continued efforts towards SAR exploitation methodologies are required (IGOS, 2007).

In this study, the well calibrated, low NESZ (–35 dB or better), and polarimetric capabilities of an in situ C-band polarimetric scatterometer (see Part 1) and the satellite RS-2 operating in Fine Quad-Pol mode, facilitated the investigation of low intensity melt pond covered FY ice. The working hypothesis, which relies on backscatter data acquired at shallow incidence angles (about 40° and higher), further exacerbated the

Sea ice melt pond fraction estimation – Part 2

R. K. Scharien

Title Page

Abstract

Introduction

Conclusions

References

Tables

Figures

◀

▶

◀

▶

Back

Close

Full Screen / Esc

Printer-friendly Version

Interactive Discussion



low intensity problem. The low intensity nature of the problem means results must be considered relative to the NESZ of SAR data sources. Co-polarisation (VV and HH) channels for the PR-based retrieval of pond fractions are not subject to noise floor contamination by RS-2, nor should they challenge the NESZ of conventional and future satellite SARs. Observed co-polarisation backscatter intensity values are approximately -20 dB or better (see Table 1). Advanced melt FY ice, irrespective of wind stress over melt ponds, does not efficiently depolarise incident microwave energy however. As such, cross-polarisation HV data, and by extension the PR_x , may be subject to noise floor contamination from SAR products outside the experimental RS-2 mode used in this study. Observed cross-polarisation backscatter intensity values are approximately -28 dB or better.

Limitations to the retrieval method include the inability to quantitatively retrieve pond fractions during ponding Stage I, due to wet snow and slush contributions to PR not accounted for by Bragg model assumptions (Sect. 2.2). The high surface permittivity state and strong PR response compared to winter does mean the timing of Ponding Stage I (i.e. pond onset) is identifiable in a seasonal series. The observed peak in PR from the SAR image series is closely associated with the timing of the Ponding Stage I peak in pond fraction and lowest ice albedo (Eicken et al., 2002; Perovich and Polashencki, 2012). This initial peak is expected to last only a few days as melt water easily made available by the shallow snow cover on undeformed sea ice is rapidly depleted. After this the surface progresses through ponding stages II and III when, as demonstrated, PR based quantitative pond fraction retrievals are tractable.

Surface cooling events also inhibit pond fraction retrievals. The formation of an ice lid on pond surfaces occurs during surface cooling periods associated with either diurnal shortwave radiation minima or, as observed with our data, longwave radiation losses related to the clearing of a low-level stratus cloud cover. The former effect is more predictable in terms of acquisition planning, as it is more likely to occur during the early local morning period associated with the descending pass of a polar-orbiting SAR. The latter effect is driven by synoptic conditions. Despite effective pond fraction

Sea ice melt pond fraction estimation – Part 2

R. K. Scharien

Title Page

Abstract

Introduction

Conclusions

References

Tables

Figures

[Back](#)

Close

Full Screen / Esc

[Printer-friendly Version](#)

Interactive Discussion



retrievals being restricted by cooling events, the resulting lack of polarization diversity and modulated PR lends itself to the identification of freeze events (i.e. surface melting state) in a seasonal series.

As defined by the frequency-dependent limiting surface roughness of the Bragg scattering model, sufficient wind stress over melt ponds is a source of uncertainty in pond fraction retrievals. When the wind stress is high enough, nominally a $U_{10} \geq 8.0 \text{ ms}^{-1}$ based on the findings in Part 1 of this study, the PR measured at C-band frequency is no longer independent of surface roughness. This represents a source of error in PR based models which depends on: the magnitude of the roughness (PR tends to unity with increasing roughness); and the relative fraction of rough patches contributing to the backscatter within a given resolution cell. A possible solution to error induced by the roughness limit lies in the utilization of lower frequency radar than C-band. L- or P-band, which effectively increases the roughness limit by way of a larger k . However, lower frequency radar may also be more sensitive to volume scattering from bare ice, which is a non-Bragg scattering process. Further investigation is required.

It is worth mentioning that, despite having fully polarimetric data for this experiment, focus was placed on the information content made available by the dual-polarisation channels only. Polarimetry is undesirable for wide-area observations of features such as sea ice, since the power requirements for polarimetric sensing restricts the available swath width during acquisition compared to dual-polarisation mode (25–50 km instead of several hundred km). This effectively limits the satellite revisit time over a given site.

6 Conclusions

Methods applicable to the retrieval of climatologically and biologically significant melt pond fraction on FY ice data using satellite C-band SAR were developed from a combination of theoretical Bragg scattering theory, in situ backscatter observations (Part 1), and satellite SAR observations (this paper, Part 2). Models based on the VV/HH polarisation ratio were developed and applied to downscaled RADARSAT-2 data of

TCD

8, 845–885, 2014

Sea ice melt pond fraction estimation – Part 2

R. K. Scharien

Title Page

Abstract

Introduction

Conclusions

References

Tables

Figures

◀

▶

◀

▶

Back

Close

Full Screen / Esc

Printer-friendly Version

Interactive Discussion



relatively undeformed FY ice in the Canadian Arctic Archipelago under variable conditions. Model performance was evaluated using aerial photography and conventional mode skill statistics (RMSE and bias), while model intercomparisons provided valuable insights into sources of uncertainty. The following objectives were addressed: (1) to synthesize calibrated dual-polarisation C-band frequency RADARSAT-2 backscatter statistics over undeformed FY ice during the ponding season, and (2) to evaluate a novel approach for the retrieval of melt pond fraction using the PR.

Our results suggest the C-band PR is suitable for the retrieval of FY ice melt pond fraction, with accuracies from a cross-validation model applied to downscaled 7.5 km PR samples comparable to optical methods. The approach provides a starting point for quantitative pond fraction mapping without the ambiguity imposed by wind forcing on pond surfaces. Where uncertainties regarding pond fraction retrievals arise, namely Ponding Stage I when wet snow is present or during cooling events, the general PR signal is better suited to the identification of the timing of these events (e.g. in a seasonal time series). The PR_x is potentially suited to pond fraction retrievals when ponds are frozen over, though no attempt was made to model this relationship as it was an isolated event. Though our test data covered the relatively small 44 to 49° incidence angle range, theoretical Bragg scattering (and in situ data in Part 1) suggest that angles as low as about 40° may be used.

In conclusion, a PR based approach provides a logical starting point for the development of robust models for quantitative estimations of sea ice melt pond parameters from SAR over various ice types, and using various radar frequencies. A bottom-up testing procedure has been presented, using data of high spatial resolution compared to the research problem. Ultimately, effective pond fraction monitoring at a much larger spatial scale is required for regional scale process studies or model based assimilations. Future work calls for development of retrievals using coarser scale, wider swath, SAR measurements combined with further examination of inter-relationships between backscatter channels and derived ratios.

Sea ice melt pond fraction estimation – Part 2

R. K. Scharien

Title Page

Abstract

Introduction

Conclusions

References

Tables

Figures

◀

▶

◀

▶

Back

Close

Full Screen / Esc

Printer-friendly Version

Interactive Discussion



Acknowledgements. This paper is dedicated to our colleague Klaus Hochheim, who lost his life in September 2013, while conducting sea ice research in the Canadian Arctic. Funding for this research was in part provided by Natural Sciences and Engineering Research Council of Canada (NSERC), the Canada Research Chairs and Canada Excellence Research Chairs programs. Randall Scharien is the recipient of a European Space Agency Changing Earth Science Network postdoctoral fellowship for the period 2013–2015. Thanks to John Yackel, and his students for use of their polarimetric scatterometer. Support was provided in the form of RADARSAT-2 data by the Canadian Space Agency's Science and Operational Applications Research (SOAR) Program, with thanks to Stephane Chalifoux. Additional RADARSAT-2 scenes were provided by the Canadian Ice Service, with thanks to Tom Zagnon and Matt Arkett. We acknowledge all participants of Arctic-ICE 2012, especially C. J. Mundy, lead investigator, and Megan Shields for assistance in the field. Gracious support for conducting aerial surveys was provided by ArcticNet and logistical support during the field campaign was provided by the Polar Continental Shelf Project (PCSP).

References

- Arrigo, K. R., Perovich, D. K., Pickart, R. S., Brown, Z. W., van Dijken, G. L., Lowry, K. E., Mills, M. M., Palmer, M. A., Balch, W. M., Bahr, F., Bates, N. R., Benitez-Nelson, C., Bowler, B., Brownlee, E., Ehn, J. K., Frey, K. E., Garley, R., Laney, S. R., Lubelczyk, L., Mathis, J., Matsuoka, A., Mitchell, B. G., Moore, G. W. K., Ortega-Retuerta, E., Pal, S., Polashenski, C. M., Reynolds, R. A., Scheiber, B., Sosik, H. M., Stephens, M., and Swift, J. H.: Massive phytoplankton blooms under Arctic sea ice, *Science*, 336, 1408, 2012.
- Barber, D. G., Papakyriakou, T. N., LeDrew, E. F., and Shokr, M. E.: An examination of the relation between the spring period evolution of the scattering coefficient (σ°) and radiative fluxes over landfast sea-ice, *Int. J. Remote Sens.*, 16, 3343–3363, 1995.
- Barber, D. G. and Yackel, J. J.: The physical, radiative and microwave scattering characteristics of melt ponds on Arctic landfast sea ice, *Int. J. Remote Sens.*, 20, 2069–2090, 1999.
- Barber, D. G.: Microwave remote sensing, sea ice and arctic climate processes, *Phys. Canada*, Sep./Oct., 61, 105–111, 2005.

Sea ice melt pond fraction estimation – Part 2

R. K. Scharien

Title Page

Abstract

Introduction

Conclusions

References

Tables

Figures

◀

▶

◀

▶

Back

Close

Full Screen / Esc

Printer-friendly Version

Interactive Discussion



Sea ice melt pond fraction estimation – Part 2

R. K. Scharien

Title Page

Abstract

Introduction

Conclusions

References

Tables

Figures

◀

▶

◀

▶

Back

Close

Full Screen / Esc

Printer-friendly Version

Interactive Discussion



- Comiso, J. C. and Kwok, R.: Surface and radiative characteristics of the summer Arctic sea ice cover from multisensor satellite observations, *J. Geophys. Res.*, 101, 28397–28416, doi:10.1029/96JC02816, 1996.
- De Abreu, R., Yackel, J. J., Barber, D. G., and Arkett, M.: Operational satellite sensing of Arctic first-year sea ice melt, *Can. J. Remote Sens.*, 27, 487–501, 2001.
- Derkson, C., J. Piwowar and LeDrew, E.: Sea-ice melt-pond fraction as determined from low level aerial photographs, *Arct. Alp. Res.*, 29(3), 345–351, 1997.
- Drinkwater, M. R.: LIMEX '87 Ice Surface Characteristics: implications for C-Band SAR backscatter signatures, *IEEE T. Geosci. Remote*, 27, 501–513, doi:10.1109/TGRS.1989.35933, 1989.
- Ehn, J. K., Mundy, C. J., Barber, D. G., Hop, H., Rossmagel, A., and Stewart, J.: Impact of horizontal spreading on light propagation in melt pond covered seasonal sea ice in the Canadian Arctic, *J. Geophys. Res.*, 116, C00G02, doi:10.1029/2010JC006908, 2011.
- Eicken, H., Krouse, H. R., Kadko, D., and Perovich, D. K.: Tracer studies of pathways and rates of meltwater transport through Arctic summer sea ice, *J. Geophys. Res.*, 107, 8046, doi:10.1029/2000JC000583, 2002.
- Eicken, H., Grenfell, T. C., Perovich, D. K., Richter-Menge, J. A., and Frey, K.: Hydraulic controls on summer Arctic pack ice albedo, *J. Geophys. Res.*, 109, C08007, doi:10.1029/2003JC001989, 2004.
- Fetterer, F. and Untersteiner, N.: Observations of melt ponds on Arctic sea ice, *J. Geophys. Res.*, 103, 24821–24835, 1998.
- Flett, D., Crevier, Y., and Girard, R.: The RADARSAT Constellation Mission: Meeting the government of Canada's needs and requirements, *Proceedings of the Geoscience and Remote Sensing Symposium, 2009 IEEE International, IGARSS 2009, Cape Town, South Africa, 12–17 July 2009*, doi:10.1109/IGARSS.2009.5418303, 2009.
- Flocco, D., Feltham, D. L., and Turner, A. K.: Incorporation of a physically-based melt pond scheme into the sea ice component of a climate model, *J. Geophys. Res.*, 115, C08012, doi:10.1029/2009JC005568, 2010.
- Freitag, J. and Eicken, H.: Meltwater circulation and permeability of Arctic summer sea ice derived from hydrological field experiments, *Ann. Glaciol.*, 49, 349–358, 2003.
- Frey, K. E., Perovich, D. K., and Light, B.: The spatial distribution of solar radiation under a melting Arctic sea ice cover, *Geophys. Res. Lett.*, 38, L22501, doi:10.1029/2011GL049421, 2011.

- Fung, A. K.: Microwave Scattering and Emission Models and Their Applications, Artech House, Inc., Norwood, Ma., 1994.
- Golden, K. M., Ackley, S. F., and Lytle, V. I.: The percolation phase transition in sea ice, *Science*, 282, 2238–2241, 1998.
- 5 Hanesiak, J. M., Yackel, J. J., and Barber, D. G.: Effect of melt ponds on first-year sea ice ablation-integration of RADARSAT-1 and thermodynamic modelling, *Can. J. Remote Sens.*, 27, 433–442, 2001a.
- Hanesiak, J. M., Barber, D. G., De Abreu, R. A., and Yackel, J. J.: Local and regional albedo observations of arctic first-year sea ice during melt ponding, *J. Geophys. Res.*, 106, 1005–1016, doi:10.1029/1999JC000068, 2001b.
- 10 Hajnsek, I., Pottier, E., and Cloude, S. R.: Inversion of surface parameters from polarimetric SAR, *IEEE T. Geosci. Remote*, 41, 727–744, 2003.
- Heygster, G., Alexandrov, V., Dybkjær, G., von Hoyningen-Huene, W., Girard-Ardhuin, F., Katsev, I. L., Kokhanovsky, A., Lavergne, T., Malinka, A. V., Melsheimer, C., Toudal Pedersen, L., Prikhach, A. S., Saldo, R., Tonboe, R., Wiebe, H., and Zege, E. P.: Remote sensing of sea ice: advances during the DAMOCLES project, *The Cryosphere*, 6, 1411–1434, doi:10.5194/tc-6-1411-2012, 2012.
- 15 Holland, M. M., Bailey, D. A., Briegleb, B. P., Light, B., and Hunke, E.: Improved sea ice short-wave radiation physics in ccs4: the impact of melt ponds and aerosols on arctic sea ice, *J. Climate*, 25, 1413–1430, doi:10.1175/JCLI-D-11-00078.1, 2012.
- Howell, S. E. L., Tivy, A., Yackel, J. J., and Scharien, R. K.: Application of a SeaWinds/QuikSCAT sea ice melt algorithm for assessing melt dynamics in the Canadian Arctic Archipelago, *J. Geophys. Res.*, 111, C07025, doi:10.1029/2005JC003193, 2006.
- IGOS Cryosphere: Integrated Global Observing Strategy (IGOS) cryosphere theme report, Geneva, Switzerland, WMO/TD-No. 1405, 102 pp., 2007.
- 25 Inoue, J., Kosovic, B., and Curry, J. A.: Evolution of a storm-driven cloudy boundary layer in the Arctic, *Bound.-Lay. Meteorol.*, 117, 213–230, 2005.
- Inoue, J., Kikuchi, T., and Perovich, D. K.: Effect of heat transmission through melt ponds and ice on melting during summer in the Arctic Ocean, *J. Geophys. Res.*, 113, C05020, doi:10.1029/2007JC004182, 2008.
- 30 Jeffries, M. O., Schwartz, K., and Li, S.: Arctic summer sea ice SAR signatures, melt season characteristics and melt pond fractions, *Polar Rec.*, 33, 101–112, 1997.

Sea ice melt pond fraction estimation – Part 2

R. K. Scharien

Title Page

Abstract

Introduction

Conclusions

References

Tables

Figures

◀

▶

◀

▶

Back

Close

Full Screen / Esc

Printer-friendly Version

Interactive Discussion



the Canadian Beaufort Sea, *Geophys. Res. Lett.*, 36, L17601, doi:10.1029/2009GL038837, 2009.

Oliver, C. and Quegan, S.: Understanding Synthetic Aperture Radar Images, SciTech Publishing, Raleigh, NC, 2004.

5 Perovich, D. K.: The optical properties of sea ice, US Army Cold Regions Research and Engineering Laboratory, Hanover, New Hampshire, Monograph 96-1, 33, 1996.

Perovich, D. K. and Polashenski, C.: Albedo evolution of seasonal Arctic sea ice, *Geophys. Res. Lett.*, 39, L08501, doi:10.1029/2012GL051432, 2012.

10 Perovich, D. K., Roesler, C. S., and Pegau, W. S.: Variability in Arctic sea ice optical properties, *J. Geophys. Res.*, 103, 1193–1208, 1998.

Perovich, D. K., Light, B., Eicken, H., Jones, K. F., Runciman, K., and Nghiem, S. V.: Increasing solar heating of the Arctic Ocean and adjacent seas, 1979–2005: attribution and role in the ice-albedo feedback, *Geophys. Res. Lett.*, 34, L19505, doi:10.1029/2007GL031480, 2007.

15 Polashenski, C., Perovich, D., and Courville, Z.: The mechanisms of sea ice melt pond formation and evolution, *J. Geophys. Res.*, 117, C01001, doi:10.1029/2011JC007231, 2012.

Pucko, M., Stern, G. A., Barber, D., Macdonald, R. W., Warner, K., and Fuchs, C.: Mechanisms and implications of α -HCH enrichment in melt pond water on Arctic sea ice, *Environ. Sci. Technol.*, 46, 11862–11869, doi:10.1021/es303039f, 2012.

20 Rösler, A., Kaleschke, L., and Birnbaum, G.: Melt ponds on Arctic sea ice determined from MODIS satellite data using an artificial neural network, *The Cryosphere*, 6, 431–446, doi:10.5194/tc-6-431-2012, 2012.

Rösler, A. and Kaleschke, L.: Exceptional melt pond occurrence in the years 2007 and 2011 on the Arctic sea ice revealed from MODIS satellite data, *J. Geophys. Res.*, 117, C05018, doi:10.1029/2011JC007869, 2012.

25 Scharien, R. K. and Yackel, J. J.: Analysis of surface roughness and morphology of first-year sea ice melt ponds: Implications for microwave scattering, *IEEE T. Geosci. Remote*, 43, 2927–2939, 2005.

Scharien, R. K., Geldsetzer, T., Barber, D. G., Yackel, J. J., and Langlois, A.: Physical, dielectric, and C band microwave scattering properties of first-year sea ice during advanced melt, *J. Geophys. Res.*, 115, C12026, doi:10.1029/2010JC006257, 2010.

30 Scharien, R. K., Yackel, J. J., Barber, D. G., Asplin, M., Gupta, M., and Isleifson, D.: Geophysical controls on C band polarimetric backscatter from melt pond covered Arctic first-year

Sea ice melt pond fraction estimation – Part 2

R. K. Scharien

Title Page

Abstract

Introduction

Conclusions

References

Tables

Figures

◀

▶

◀

▶

Back

Close

Full Screen / Esc

Printer-friendly Version

Interactive Discussion



sea ice: assessment using high-resolution scatterometry, *J. Geophys. Res.*, 117, C00G18, doi:10.1029/2011JC007353, 2012.

Skyllingstad, E. D., Pauson, C. A., and Perovich, D. K.: Simulation of melt pond evolution on level ice, *J. Geophys. Res.*, 114, C12019, doi:10.1029/2009JC005363, 2009.

5 Soluri, E. A. and Woodson, V. A.: World Vector Shoreline, International Hydrographic Review, International Hydrographic Organization, Monaco, LXVII, 1990.

Taylor, P. D. and Feltham, D. L.: A model of melt pond evolution on sea ice, *J. Geophys. Res.*, 109, C12007, doi:10.1029/2004JC002361, 2004.

10 Torres, R., Snoeij, P., Geudtner, D., Bibby, D., Davidson, M., Attema, E., Potin, P., Rommen, B.,
Floury, N., Brown, M., Navas Traver, I., Deghaye, P., Duesmann, B., Rosich, B., Miranda, N.,
Bruno, C., L'Abbate, M., Croci, R., Pietropaolo, A., Huchler, M., F. Rostan: GMES Sentinel-1
mission, *Remote Sens. Environ.*, 120, 9–24, doi:10.1016/j.rse.2011.05.028, 2012.

15 Tschudi, M. A., Curry, J. A., and Maslanik, J. A.: Airborne observations of summertime surface features and their effect on surface albedo during FIRE/SHEBA, *J. Geophys. Res.*, 106, 15335–15344, doi:10.1029/2000JD900275, 2001.

Tschudi, M. A., Maslanik, J. A., and Perovich, D. K.: Derivation of melt pond coverage on Arctic sea ice using MODIS observations, *Remote Sens. Environ.*, 112, 2605–2614, 2008.

Ulaby, F. T., Moore, R. K., and Fung, A. K.: *Microwave Remote Sensing: Active and Passive. From Theory to Applications*, Vol. III, Artech House, Inc., Norwood, Massachusetts., 1986.

20 Vachon, P. W. and Wolfe, J.: C-Band cross-polarization wind speed retrieval, *Geosci. Remote Sens. Lett.*, 8, 451–455. doi:10.1109/LGRS.2010.2085417, 2011.

Vancoppenolle, M., Meiners, K. M., Michel, C., Bopp, L., Brabant, F., Carnat, G., Delille, B., Lannuzel, D., Madec, G., Moreau, S., Tison, J.-L., and van der Merwe, P.: Role of sea ice in global biogeochemical cycles: emerging views and challenges, *Quat. Sci. Rev.*, 79, 207–230, doi:10.1016/j.quascirev.2013.04.011, 2013.

Yackel, J. J. and Barber, D. G.: Melt ponds on sea ice in the Canadian Archipelago 2. On the use of RADARSAT-1 synthetic aperture radar for geophysical inversion, *J. Geophys. Res.-Oceans*, 105, 22061–22069, 2000.

30 Yackel, J.J, Barber, D. G., and Hanesiak, J. M.: Melt ponds on sea ice in the Canadian Archipelago 1. Variability in morphological and radiative properties, J. Geophys. Res., 105, 22049–22060, 2000.

Zege, E., Katsev, I., Malinka, A., Prikhach, A., and Heygster, G.: New approach for radiative transfer in sea ice and its application for sea ice satellite remote sensing, radiative transfer in sea ice, 2017.

8, 845–885, 2014

Sea ice melt pond fraction estimation – Part 2

R. K. Scharien

Title Page

Abstract

Introduction

Conclusions

References

Tables

Figures



[Back](#)

Close

Full Screen / Esc

[Printer-friendly Version](#)

Interactive Discussion



TCD

8, 845–885, 2014

Sea ice melt pond
fraction estimation –
Part 2

R. K. Scharien

Title Page

Abstract

Introduction

Conclusions

References

Tables

Figures



Back

Close

Full Screen / Esc

Printer-friendly Version

Interactive Discussion



Sea ice melt pond fraction estimation – Part 2

R. K. Scharien

Table 1. Radarsat-2 scene characteristics, nearest coincident hourly air temperature (T_a , in $^{\circ}\text{C}$) and wind speed (U_{10} , in m s^{-1}) recorded at Resolute Airport, and HH, VV and HV polarisation backscatter and polarisation ratios (dB) after SAR processing.

ID	Site	Date and time	Pass	IA $^{\circ}$	T_a $^{\circ}\text{C}$	U_{10} m s^{-1}	F_{pond}	VV dB	HH dB	HV dB	PR dB	PR _x dB
[R1]	Parry	12 May 2012 12:51	Des	49	−7.7	5.6		−22.5	−22.4	−29.4	−0.1	−7.0
[R2]	Parry	13 Jun 2012 23:54	Asc	44	3.9	11.9	0.38	−16.0	−20.1	−28.0	4.1	−7.9
[R3]	Field	20 Jun 2012 23:50	Asc	44	0.8	4.7	0.53	−15.6	−18.2	−26.8	2.6	−8.6
[R4]	Parry	24 Jun 2012 00:02	Asc	47	4.6	5.3	0.55	−17.4	−18.7	−27.0	1.3	−8.3
[R5]	Parry	29 Jun 2012 12:51	Des	49	5.1	1.1	0.39	−16.7	−18.4	−26.5	1.7	−8.1

[Title Page](#)
[Abstract](#)
[Introduction](#)
[Conclusions](#)
[References](#)
[Tables](#)
[Figures](#)
[◀](#)
[▶](#)
[◀](#)
[▶](#)
[Back](#)
[Close](#)
[Full Screen / Esc](#)
[Printer-friendly Version](#)
[Interactive Discussion](#)


Sea ice melt pond fraction estimation – Part 2

R. K. Scharien

Title Page

Abstract

Introduction

Conclusions

References

Tables

Figures

◀

▶

◀

▶

Back

Close

Full Screen / Esc

Printer-friendly Version

Interactive Discussion



Table 2. Relationships between measured and retrieved pond fraction from RADARSAT-2 scenes R2 to R5, using three retrieval methods.

Model	Mission	RMSE	Bias
Cscat	R2	0.44	0.41
	R3	0.07	−0.02
	R4	0.27	−0.25
	R5	0.15	−0.13
Bragg	R2	0.53	0.50
	R3	0.07	0.03
	R4	0.25	−0.22
	R5	0.11	−0.09
Cross-val.	R2	0.37	0.34
	R3	0.07	0.00
	R4	0.17	−0.12
	R5	0.07	0.01

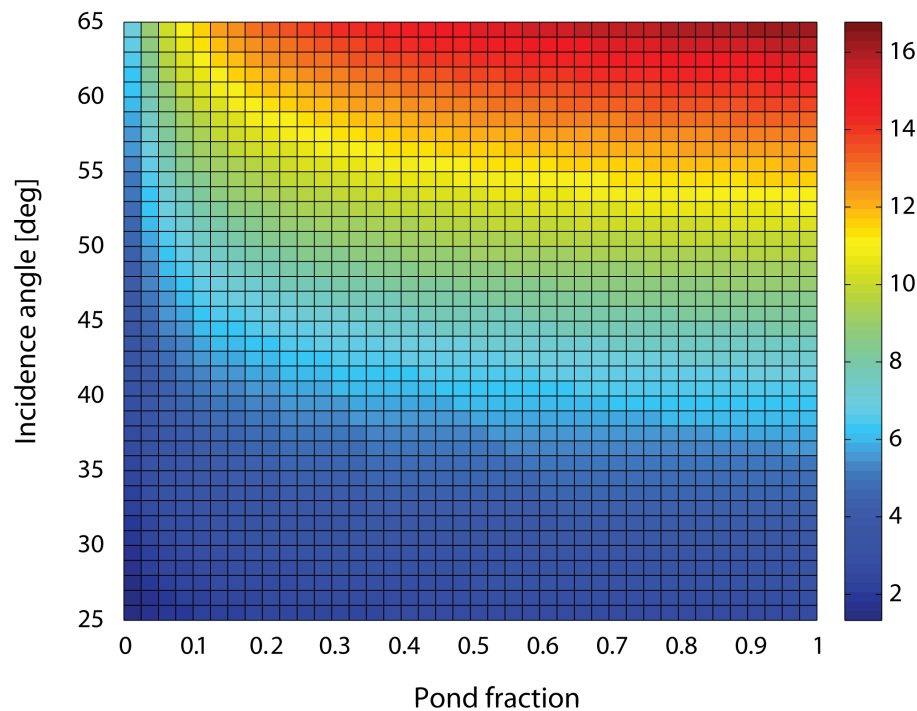


Fig. 1. Polarisation ratio (PR) intensity in decibels (dB) of a first-year sea ice cover as a function of increasing radar incidence angle and melt pond fraction, estimated using the Bragg model.

Sea ice melt pond fraction estimation – Part 2

R. K. Scharien

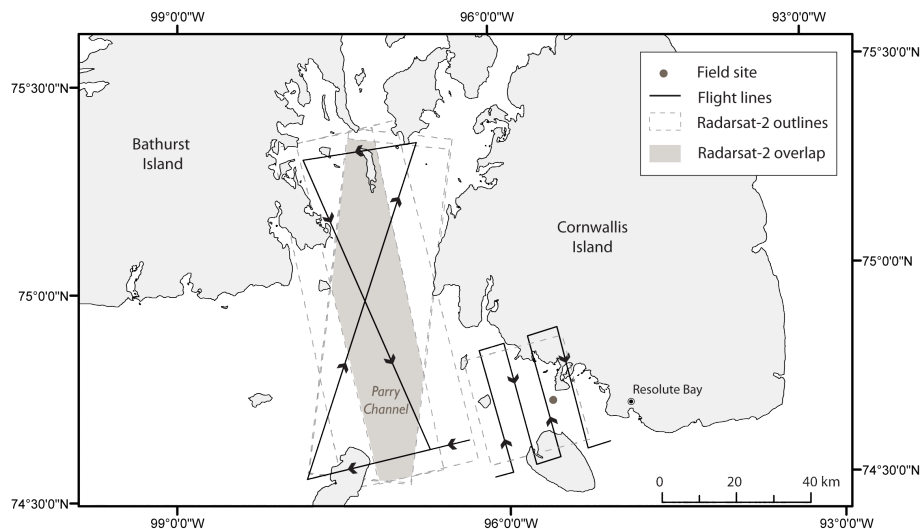


Fig. 2. Map showing location of field site adjacent to the hamlet of Resolute Bay, NU in the central Canadian Arctic Archipelago. Aerial photography flight lines over *Parry* and *Field* locations are shown along with outlines of 75 by 25 km (*Parry*) and 25 by 25 km (*Field*) RADARSAT-2 scenes. The shaded region over Parry denotes the overlapping portion of scenes acquired over the site.

Title Page

Abstract

Introduction

Conclusions

References

Tables

Figures

◀

▶

◀

▶

Back

Close

Full Screen / Esc

Printer-friendly Version

Interactive Discussion



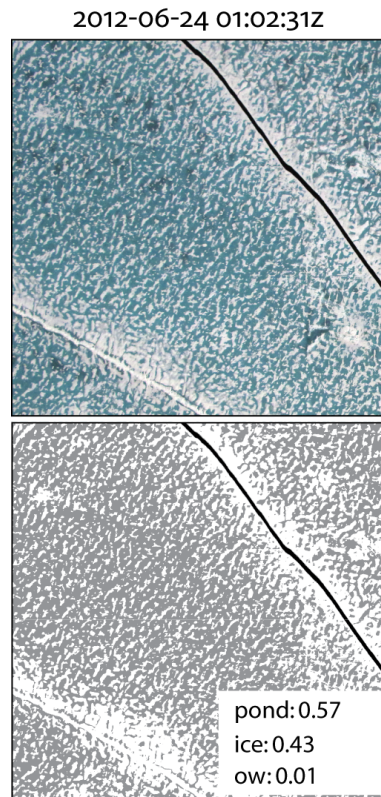


Fig. 3. Exemplative 900 by 900m aerial photo from Parry site on 24 June 2012 (top) and decision-tree classification result with ponds in grey, ice in white, and open water in black (bottom). Relative fractions of each cover type are given at the bottom.

Sea ice melt pond fraction estimation – Part 2

R. K. Scharien

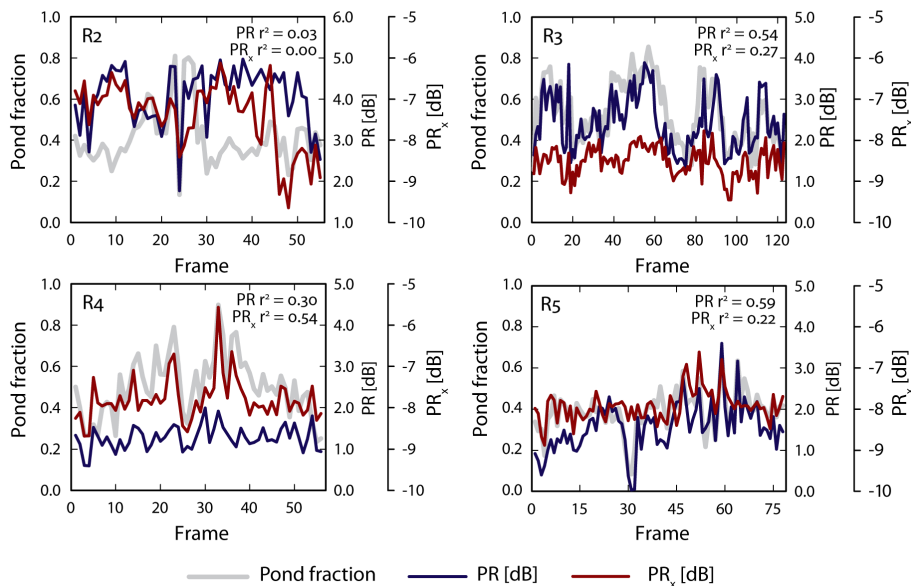


Fig. 4. Polarimetric ratios PR and PR_x from RADARSAT-2 scenes R2 to R5, shown along with coincident measured melt pond fractions from partitioned aerial photos. Coefficients of determination between each polarimetric ratio and pond fraction are given.

Title Page

Abstract

Introduction

Conclusions

References

Tables

Figures

◀

▶

◀

▶

Back

Close

Full Screen / Esc

Printer-friendly Version

Interactive Discussion



Sea ice melt pond
fraction estimation –
Part 2

R. K. Scharien

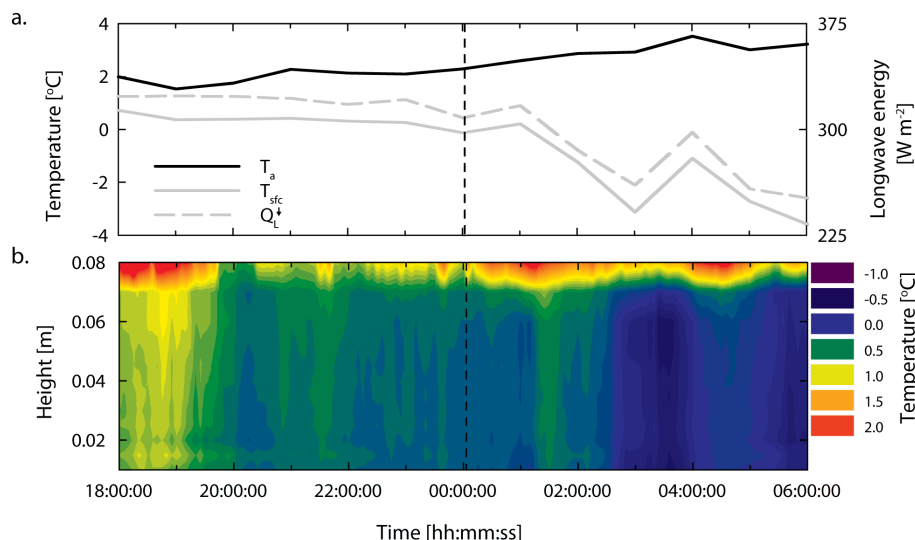


Fig. 5. Meteorological variables and melt pond water temperature profile from 23 June 2012 18:00:00 Z to 24 June 2012 06:00:00 Z at the Field site, with the time of the R4 acquisition and coincident AP survey indicated by dashed vertical lines. **(a)** 1 m air temperature (T_a), surface temperature (T_{sfc}), and downwelling longwave radiation (Q_L^{\downarrow}). **(b)** Temperature profile of a melt pond. The pond water level was recorded as 0.085 m before, and 0.075 m after, the time series. The absolute position of the air–water interface varied due to competing melt water formation and drainage processes, and surface waves.

Title Page

Abstract

Introduction

Conclusions

References

Tables

Figures

◀

▶

◀

▶

Back

Close

Full Screen / Esc

Printer-friendly Version

Interactive Discussion



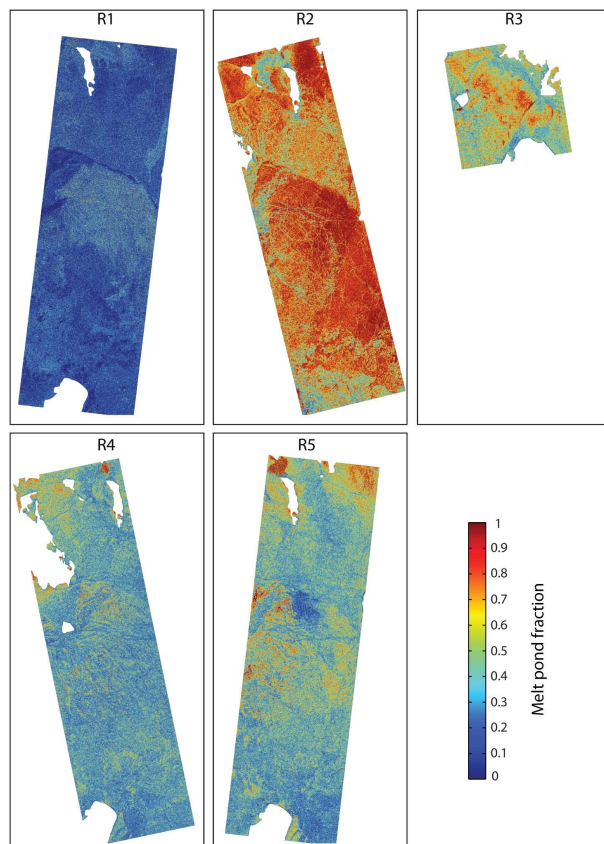


Fig. 6. Retrieved melt pond fraction using the cross-validation retrieval method. Refer to the map provided in Fig. 2 for scale and location information and Table 1 for information regarding scenes R1 to R5.

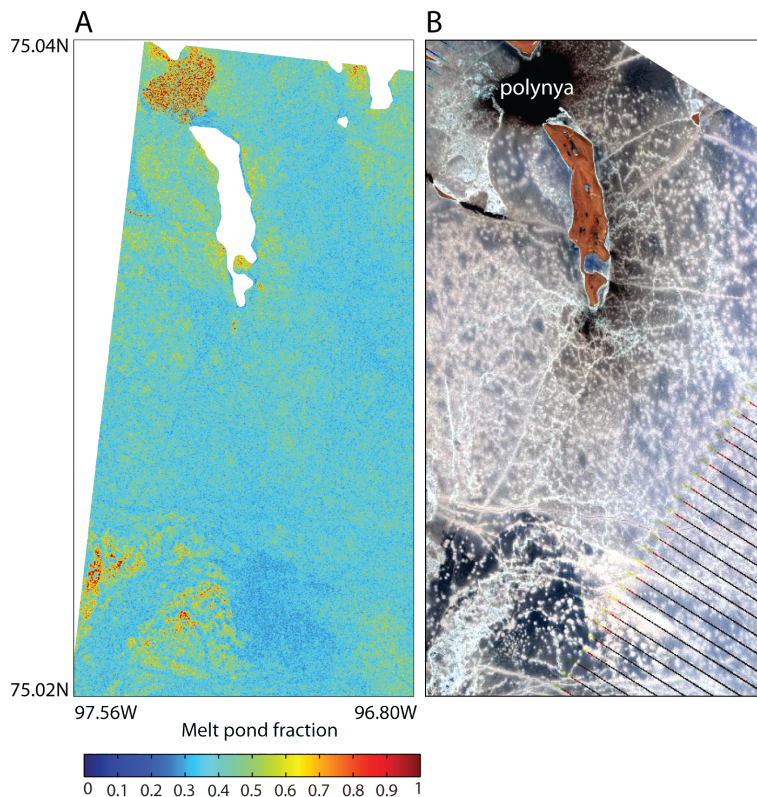


Fig. 7. (a and b) Comparison between the retrieved melt pond fraction from R5 (refer Table 1) and an RGB colour-composite created by combining Bands 4, 3, and 2 from a Landsat-7 ETM+ satellite image acquired on the same day. Dark lines visible in the bottom right portion of the Landsat-7 scene are due to the instrument Scan Line Corrector (SLC) failure.

Sea ice melt pond fraction estimation – Part 2

R. K. Scharien

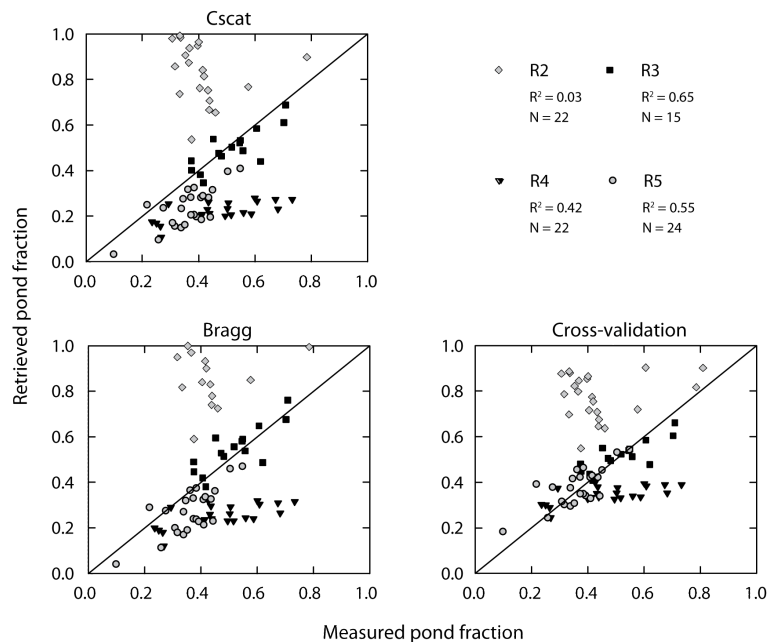


Fig. 8. Comparison of different retrieval methods for the inversion of melt pond fraction from RADARSAT-2 scenes R2 to R5.

[Title Page](#)[Abstract](#)[Introduction](#)[Conclusions](#)[References](#)[Tables](#)[Figures](#)[◀](#)[▶](#)[◀](#)[▶](#)[Back](#)[Close](#)[Full Screen / Esc](#)[Printer-friendly Version](#)[Interactive Discussion](#)